# The Regional Climate-Chemistry-Ecology Coupling Model RegCM-Chem (v4.6)-YIBs (v1.0): Development and Application

Nanhong Xie[1], Tijian Wang[1]*, Xiaodong Xie[2], Xu Yue[2], Filippo Giorgi[3], Qian Zhang[1], Danyang Ma[1], Rong Song[1], Beiyao Xu[1], Shu Li[1], Bingliang Zhuang[1], Mengmeng Li[1], Min Xie[1], Natalya Andreeva Kilifarska[4], Georgi Gadzhev[5], Reneta Dimitrova[6]

[1]School of Atmospheric Sciences, Nanjing University, Nanjing, 210023, China

[2]School of Environmental Sciences and Engineering, Nanjing University of Information Science and Technology, Nanjing, 210023, China

[3]Earth System Physics Section, the Abdus Salam International Centre for Theoretical Physic, Trieste, 34100, Italy

[4]Climate, Atmosphere and Waters Research Institute, Bulgarian Academy of Sciences, Sofia, 1113, Bulgaria

[5]National Institute of Geophysics, Geodesy and Geography, Bulgarian Academy of Sciences, Sofia, 1113, Bulgaria

[6]Department of Meteorology and Geophysics, Faculty of Physics, Sofia University, Sofia, 1113, Bulgaria

*Corresponding to*: Tijian Wang (tjwang@nju.edu.cn)

**Abstract.** The interactions between the terrestrial biosphere, atmospheric chemistry, and climate involve complex feedbacks that have traditionally been modeled separately. We present a new framework that couples the Yale Interactive terrestrial Biosphere (YIBs), a dynamic plant-chemistry model, with the RegCM-Chem model. RegCM-Chem-YIBs integrates meteorological variables and atmospheric chemical composition from RegCM-Chem with land surface parameters from YIBs. The terrestrial carbon flux calculated by YIBs, are fed back into RegCM-Chem interactively, thereby representing the interactions between fine particulate matter ($PM_{2.5}$), ozone ($O_3$), and carbon dioxide ($CO_2$). For testing purposes, we carry out a one-year simulation (2016) at a 30 km horizontal resolution over East Asia with RegCM-Chem-YIBs. The model accurately captures the spatio-temporal distribution of climate, chemical composition, and ecological parameters. In particular, the estimated $O_3$ and $PM_{2.5}$ are consistent with ground observations, with correlation coefficients (R) of 0.74 and 0.65, respectively. The simulated $CO_2$ concentration is consistent with observations from six sites (R ranged from 0.89 to 0.97) and exhibits a similar spatial pattern when compared to carbon assimilation products. RegCM-Chem-YIBs produces reasonably good gross primary productivity (GPP) and net primary productivity (NPP), showing seasonal and spatial distributions consistent with satellite observations, and mean biases (MBs) of 0.13 and 0.05 kg C m$^{-2}$ year$^{-1}$. This study illustrates that the RegCM-Chem-YIBs is a valuable tool to investigate coupled interactions between the terrestrial carbon cycle, atmospheric chemistry, and climate change at a higher resolution in regional scale.

## 1 Introduction

Air pollution and climate change are major focal points in atmospheric and environmental science (Hong et al., 2019; Kan et al., 2012). In this respect, China exhibits both high air pollution levels and large greenhouse gas emissions (Zheng et al., 2018; Li et al., 2016a). The consequences of China's air pollution on global, regional, and urban climate are significant (Liu et al., 2022; Lu et al., 2020). Conversely, global warming impacts the dynamics, physics, and chemical mechanisms underlying atmospheric pollutant formation, underscoring a robust link between atmospheric chemistry and climate change (Baklanov et al., 2016; Fiore et al., 2015; Fiore et al., 2012).

$PM_{2.5}$, $O_3$, and $CO_2$ are important for regional air pollution and climate. $O_3$, a potent pollutant, is harmful for human health and can also harm chloroplasts in plant cells, consequently influencing the carbon assimilation efficiency of land ecosystems (Xie et al., 2019; Ainsworth et al., 2012). Similarly, $PM_{2.5}$ is not only one of the most dangerous pollutants for human health (Kim et al., 2015), but also affects atmospheric radiation mechanics, modulates radiation fluxes reaching vegetation canopies, and hence impacts plant physiological processes and terrestrial carbon fluxes (Lu et al., 2017; Strada and Unger, 2016). Terrestrial ecosystems, absorbing nearly 30% of anthropogenic $CO_2$ emissions, play an essential role in the global carbon cycle, for which even minor alterations can trigger significant oscillations in atmospheric $CO_2$ concentrations, potentially destabilizing the global climate (Forkel et al., 2016; Ahlstrom et al., 2015). As a result, $PM_{2.5}$, $O_3$, and $CO_2$ exhibit intricate interplays.

Models that couple climate and chemistry are vital tools for investigating the interplay between environmental pollution and climate warming (Dunne et al., 2020; Yahya et al., 2017), and in particular the direct and indirect influences of aerosols, $O_3$, and greenhouse gases on climates at different scales (Chutia et al., 2019; Pu et al., 2017; Li et al., 2017a). For example, the Atmospheric Chemistry and Climate Model Intercomparison Project (ACCMIP) addresses this issue through the use of a range of global coupled climate-chemistry models (Young et al., 2013; Shindell et al., 2013; Lamarque et al., 2013). In fact, China has achieved significant advancements in atmospheric chemistry and coupled climate models during recent years, both at the global and regional scale. Representative models encompass BCC_AGCM2.0_CAM, BCC-AGCM_CUACE2.0, RIEMS-Chem, and RegCCMS.

BCC_AGCM2.0_CAM was coupled by the China Meteorological Administration through direct integration of the National Climate Center's atmospheric circulation model (BCC-AGCM) with the Canadian aerosol model (CAM) (Zhang et al., 2012). Atmospheric model BCC-AGCM2.0 was developed by the National Climate

62    Center. For example, at the regional scale the Institute of Atmospheric Physics of the Chinese Academy of Sci-

63    ences, has constructed the Regional Integrated Environmental Modeling System (RIEMS), which is widely used

64    in studies on East Asian regional climate change and severe weather systems (Scheuch et al., 2015; Xiong et al.,

65    2009). It incorporates atmospheric chemistry and aerosol dynamics into the Regional Integrated Environment

66    Modeling System and produces online simulations of meteorological parameters, aerosol chemical composition,

67    optical characteristics, radiation forcing, and aerosol-induced climate feedback (Li et al., 2014; Li et al., 2013a;

68    Han et al., 2012).

69    The Nanjing University developed the Regional Climate Chemistry Modeling System (RegCCMS), a syn-

70    thesis of the regional climate model RegCM2 and the tropospheric atmospheric chemistry model TACM, pri-

71    marily oriented toward investigating the spatio-temporal distribution, radiation forcing, and climatic effects of

72    tropospheric $O_3$ and sulfate aerosols. Subsequently, RegCM3 was coupled with TACM, integrating modules for

73    aerosols into RegCCMS (Zhang et al., 2014; Li et al., 2009). The system incorporates parameterization schemes

74    facilitating the simulation of aerosols' direct, indirect, and semidirect climatic effects. Extensive evaluations

75    have been carried out regarding major aerosol impacts on the meteorology and regional climate within East Asia

76    (Zhuang et al., 2013; Zhuang et al., 2011; Wang et al., 2010). Subsequently, Shalaby et al. (2012) developed the

77    regional climate-chemistry model RegCM-Chem, by coupling the CBM-Z gas phase chemistry module to ver-

78    sion 4 of the RegCM system, RegCM4 (Giorgi et al., 2012). RegCM-Chem also includes a simplified aerosol

79    scheme including radiatively interactive sulfates, carbonaceous aerosols, sea salt, and desert dust (Zakey et al.,

80    2006; Solmon et al., 2006), and it has been used for a variety of applications in different domains.

81    By developing the regional climate-chemistry-ecology model RegCM-Chem-YIBs, in which the interactive

82    biosphere model YIBs is coupled to RegCM-Chem. The model can produce multi-process simulations of re-

83    gional climate, atmospheric chemistry, and ecology, especially $PM_{2.5}$, $O_3$, and $CO_2$, and their interactions with

84    atmospheric variables (Xu et al., 2023; Ma et al., 2023b; Ma et al., 2023a; Xu et al., 2022; Gao et al., 2022; Xie

85    et al., 2020). Here we expand on these previous studies. We carry out a one-year simulation (2016) at a 30 km

86    horizontal resolution over East Asia with RegCM-Chem-YIBs and conduct a comprehensive assessment. We

87    validate the simulation not only in terms of atmospheric variables but also in terms of atmospheric composition

88    and ecological parameters, by comparison with a range of observations available for this period.

89    The paper is organized as follows. In section 2 we first describe the RegCM-Chem-YIBs system, focusing

90    in particular on the newly implemented coupling with the ecological component. We also describe the observa-

91  tion datasets used in the model assessment. The simulations are then analyzed in section 3, while section 4 pre-

92  sents our conclusions and a general discussion of our results and future developments.

93  **2 Model and Methods**

94  **2.1 Overall Framework**

95      In RegCM-Chem-YIBs, the atmospheric variables produced by RegCM (temperature, humidity, precipita-

96  tion, radiation, etc.) and atmospheric chemical compounds, such as $O_3$ and $PM_{2.5}$, produced by the chemis-

97  try/aerosol module are input into YIBs, which simulates the physiological processes of vegetation (such as pho-

98  tosynthesis, respiration, etc.), and calculates land process variables such as $CO_2$ fluxes, BVOC emissions, and

99  stomatal conductance. The output from YIBs is then fed back to RegCM-Chem, which adjusts the $CO_2$, $O_3$, and

100  $PM_{2.5}$ concentrations and their radiative and microphysical effects on the meteorological fields in the lower at-

101  mosphere, thereby achieving a full coupling between climate, chemistry, and ecology. Figure 1 shows the basic

102  framework of the RegCM-Chem-YIBs coupled model.
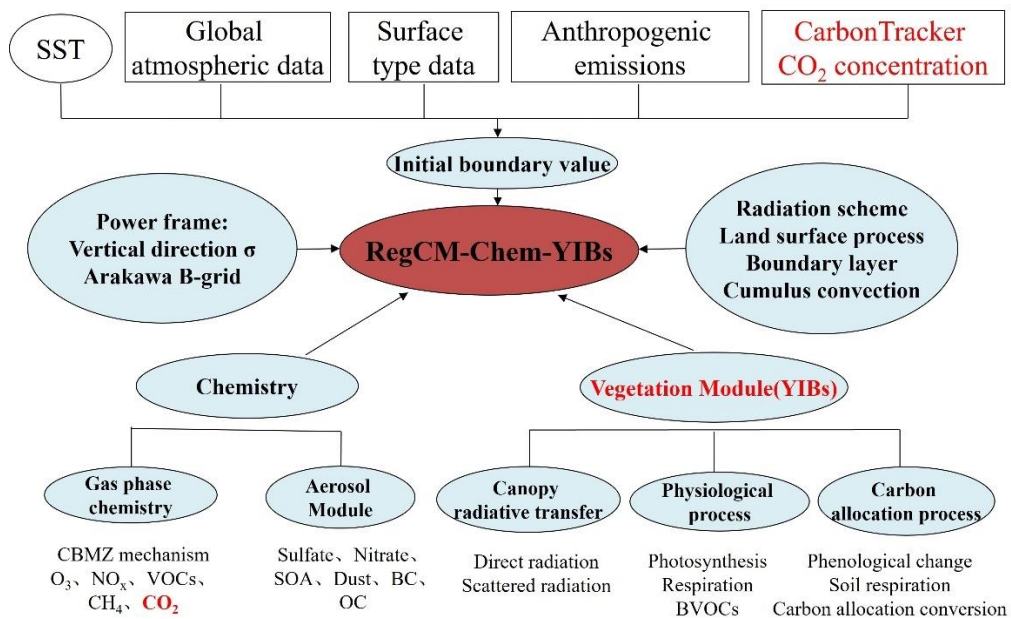
103



104  **Figure 1.** RegCM-Chem-YIBs Coupling Model Framework

105  **2.2 Descriptions of the RegCM-Chem model**

106      The inception of the RegCM system traces back to the late 1980s and early 1990s, when NCAR's (U.S. Na-

107  tional Center for Atmospheric Research) RegCM 1 was first developed for climate downscaling (Giorgi, 1990;

108 Giorgi and Bates, 1989; Dickinson et al., 1989). After a series of developments, subsequent versions were in-

109 troduced, such as RegCM2 (Giorgi et al., 1993), RegCM2.5 (Giorgi and Mearns, 1999), RegCM3 (Pal et al.,

110 2007), RegCM4 (Giorgi et al., 2012). The RegCM system presently managed, maintained, and expanded by the

111 Earth System Physics (ESP) section of the Abdus Salam International Center for Theoretical Physics (ICTP), is

112 open-source and extensively employed in regional climate studies, contributing to the establishment of a com-

113 prehensive Regional Climate Research Network (RegCNET) (Giorgi et al., 2006). The model can be applied to

114 all regions of the globe (Giorgi et al., 2012) and is moving into a fully-coupled regional Earth system model

115 framework through coupling with the ocean (Turuncoglu et al., 2013; Artale et al., 2010), lake (Small et al.,

116 1999), aerosol (Solmon et al., 2006), dust (Zakey et al., 2006), chemistry (Shalaby et al., 2012), hydrology

117 (Coppola et al., 2003), land surface processes (Oleson et al., 2008). Of specific interest for our study, Shalaby et

118 al. (2012) added a radiatively interactive gas-phase chemical module (CBM-Z) to RegCM4, generating

119 RegCM-Chem, in which atmosphere physics and chemistry are fully coupled.

120 **2.2.1 Aerosol Mechanisms**

121  The RegCM model integrates a simplified aerosol framework, enabling the simulation of sulfate, black

122 carbon (BC), organic carbon (OC), sea salt, and desert dust. The model specifies an external mix of aerosols and

123 accounts for the influence of horizontal advection, turbulent diffusion, vertical transport, emissions, dry and wet

124 deposition, and gas-liquid transition on aerosol concentration (Solmon et al., 2012; Giorgi et al., 2012; Zakey et

125 al., 2006). The secondary organic aerosol scheme VBS (volatile basis set) has also been introduced into the

126 model to further improve RegCM-Chem's simulation of tropospheric aerosols (Yin et al., 2015). The model in-

127 corporates the ISORROPIA thermodynamic equilibrium scheme to describe the formation process of secondary

128 inorganic salts, thus enhancing the model's capability to simulate secondary inorganic aerosols (Li et al., 2016b).

129 The further addition of bioaerosols was carried out by Liu (Liu et al., 2016).

130 **2.2.2 Gas phase chemical mechanism**

131  RegCM4-Chem includes the CBM-Z (Carbon Bond Mechanism-Z) atmospheric chemistry mechanism

132 (Zaveri and Peters, 1999). The CBM-IV mechanism, recognized for its widespread use, serves as the basis for

133 CBM-Z (Gery et al., 1989) and was developed to balance simulation accuracy and computational speed. Both

134 CBM-IV and CBM-Z categorize volatile organic compounds (VOCs) into groups dependent on their carbon

135 bond formation and use lumped species to represent each group. However, CBM-Z includes additional species

136 and reactions compared to CBM-IV, which are crucial for simulating typical urban environments and long-term

137 simulations at regional to global scales. Enhancements in CBM-Z include (1) specific representation of stable

138 alkanes; (2) updated parameters for higher alkanes; (3) separation of olefins into two categories based on differ-

139 ing reactions; (4) addition of peroxy alkane self-reactions significant in low-NOx, such as remote regions; (5)

140 incorporation of reactions among alkanes, peroxyacyl radicals, and $NO_3$, which are crucial nocturnally; (6) in-

141 clusion of long-lived organic nitrates and peroxides; and (7) refinement of isoprene and its peroxy radical chem-

142 istry. Collectively, these updates to the CBM-Z chemistry mechanism enhance the model's ability to more accu-

143 rately simulate long-lived VOCs and address the atmospheric chemistry transition from urban to rural settings.

144 **2.2.3 Radiation scheme**

145 RegCM4 adopts the CCM3 radiation scheme, which uses the delta-Eddington approximation for solar

146 spectral radiation and accounts for the attenuation effect of atmospheric components such as $O_3$, $H_2O$, $CO_2$, $O_2$

147 on solar radiation (Kiehl et al., 1996). The CCM3 radiation scheme, implemented in RegCM4, extends from 0.2

148 to 5 µm, and is segmented into 18 bands. It uses the cloud scattering and absorption parameter scheme, and

149 cloud optical characteristics. As cumulus clouds form, the cloud optical characteristics stretch from the cloud

150 base up to the cloud top, and the radiation calculations assume random overlap. It is assumed in the model that

151 the cloud thickness is equivalent to that of the model's vertical layers, with distinctive cloud water and ice

152 contents assigned to high, middle, and low clouds (Slingo, 1989).

153 **2.2.4 Photolysis rate**

154 Meteorological conditions and chemical input fields determine the photolysis rate, with most variables

155 dynamically produced by the RegCM's modules and updated every 3-30 minutes. $SO_2$ and NOx, inverted from

156 the US standard atmosphere's vertical profile, are model-defined. Owing to the computational demands of

157 precise photolysis rates from the Tropospheric Ultraviolet–Visible Model (TUV) method (Madronich and

158 Flocke, 1998) and eight data stream spherical harmonics discretization, a look-up table and interpolation method

159 are adopted. Considering the significant impact of clouds on the photolysis rate, it becomes crucial to adjust the

160 cloud amount. Here we use the cloud optical depth information for each grid cell within the model. As the

161 absorption and scattering of ultraviolet radiation by clouds reduce the photolysis rate inside and below the cloud

162 while enhancing it above the cloud, the correction value for the photolysis rate under clear sky conditions de-

163 pends on the position to the cloud layer. Hence, cloud height and optical depth are necessary for the photolysis

164 rate computation (Chang et al., 1987).

165 **2.2.5 Deposition Processes**

166 In the model, dry deposition serves as the principal removal process for trace gases, with the deposition

167 velocity being determined by three categories of resistance: aerodynamic, quasi-laminar sublayer, and surface

168 resistance, encompassing soil and vegetation absorption. The latter is inclusive of both stomatal and nonstomatal

169 absorption. The dry deposition module, taken from the CLM4 surface scheme, covers 29 gas-phase species and

170 comprises 11 types of land cover. To enhance the accuracy of the daily variation in dry deposition simulation,

171 both stomatal and nonstomatal resistances are accounted for in the dry deposition scheme. The calculation of all

172 deposition resistances is performed within the CLM land surface model (Wesely, 1989). Wet deposition uses the

173 MOZART global model's wet deposition parameterization scheme (Emmons et al., 2010; Horowitz et al., 2003),

174 including 26 gas-phase species in CBM-Z, and the wet deposition amount is based on the simulated precipita-

175 tion.

176 **2.3 Descriptions of the YIBs model**

177 The YIBs model, pioneered by Yale University, integrates plant physiological mechanisms to simulate how

178 photosynthesis, respiration, and other physiological processes respond to environmental drivers such as radia-

179 tion, temperature, and moisture. Moreover, YIBs simulates the carbon cycle both regionally and globally (Yue

180 and Unger, 2015). For example, its simulation of terrestrial carbon flux closely matches ground flux observa-

181 tions and satellite-derived data in diverse geographical areas such as the United States and China (Yue and

182 Unger, 2017; Yue et al., 2017).

183 **2.3.1 The main processes in YIBs**

184 In the YIBs model, eight distinct Plant Functional Types (PFTs) are incorporated, encompassing evergreen

185 coniferous forest, evergreen broad-leaved forest, deciduous broad-leaved forest, shrub forest, tundra, C3 grass-

186 land, C4 grasslands, and crops. The model employs the Michaelis–Menten enzyme-kinetics scheme for simulat-

187 ing plant photosynthesis (Farquhar et al., 1980), and the total photosynthesis ($A_{tot}$) of leaves is affected by Ru-

bisco enzyme activity ($J_c$), electron transfer rate ($J_e$), and photosynthetic product (triose phosphate) transport

capacity ($J_S$) limitation.

**2.3.2 Canopy Radiation Scheme**

A multilayer canopy radiation transmission scheme is adopted in YIBs for canopy radiation transmission

(Spitters et al., 1986), consisting of a radiation transfer model based on the total leaf area index, extinction coef-

ficient, and vegetation height. The entire vegetation canopy is usually divided into 2 to 16 layers, and the spe-

cific number of layers can be automatically adjusted according to the height of the canopy.

**2.3.3 Biogenic Volatile Organic Compound Emission Scheme**

Differently from the traditional MEGAN scheme, the YIBs model applies a biogenic volatile organic com-

pound (BVOC) emission scheme on a leaf scale, which is better suited to describe the photosynthesis process in

vegetation (Guenther et al., 1995). This introduces an effect of plant photosynthesis on BVOC emissions which

is more closely related to the real physiological process of vegetation. BVOC emissions from leaves to the can-

opy are integrated to obtain total canopy emissions. The intensity of leaf BVOC emission depends on the rate of

photosynthesis $J_e$ under electron transfer rate limitation, leaf surface temperature, and intracellular $CO_2$ con-

centration (Yue and Unger, 2015):

$$I = J_e \cdot \beta \cdot \kappa \cdot \tau \cdot \varepsilon , \qquad (1)$$

where I is the intensity of leaf BVOC emission in units of μmol m$^{-2}$[leaf] s$^{-1}$. $J_e$ is the electron

transport-limited photosynthesis rate, the calculation formula is as follows:

$$J_e = a_{leaf} \cdot PAR \cdot \alpha_{qe} \cdot \frac{C_i - \Gamma^*}{C_i - 2\Gamma^*} , \qquad (2)$$

where $a_{leaf}$ is the leaf-specific light absorbance, PAR is photosynthetically active radiation, $\alpha_{qe}$ is the intrin-

sic quantum efficiency for photosynthetic $CO_2$ uptake in the chlorophyll reaction system. $C_i$ is the internal leaf

$CO_2$ concentration. $\Gamma^*$ is the $CO_2$ concentration compensation point in the absence of non-photorespiratory

respiration (Collatz et al., 1991).

$\beta$ is the coefficient for converting electron transfer flux into BVOC emissions (Niinemets et al., 1999;

Pacifico et al., 2011):

$$\beta = \frac{C_i - \Gamma^*}{6(4.67C_i + 9.33\Gamma^*)} , \qquad (3)$$

where $\kappa$ is related to the internal leaf $CO_2$ concentration:

$$\kappa = \frac{C_{i\_standard}}{C_i}, \qquad (4)$$

where $C_{i\_standard}$ is the internal leaf $CO_2$ concentration under standard conditions (when atmospheric $CO_2$ is 370 ppm). The $\tau$ term reflects the response of BVOC emission intensity to temperature:

$$\tau = \exp[0.1(T - T_{ref})]. \qquad (5)$$

where T is the blade surface temperature, $T_{ref}$ is the standard temperature (30 °C). When the blade temperature is 40 °C, the BVOC emission intensity is maximum. As the temperature further rises, the BVOC emission gradually weakens. In reality, such high temperatures are relatively rare and may only occur under extremely dry climate conditions.

### 2.3.4 Ozone Damage Protocol

When tropospheric ozone enters plants through stomata, it can directly damage plant cell tissues, thereby slowing the photosynthesis rate and further weakening the carbon sequestration capacity of vegetation. The YIBs model incorporates the semi-mechanistic parameterization scheme to delineate ozone's effect on plants (Sitch et al., 2007):

$$A = A_{tot} \cdot F, \qquad (6)$$

where A is photosynthesis minus the influence of ozone, $A_{tot}$ is the total photosynthesis of leaves, F is the proportion of photosynthesis minus the influence of ozone, which depends on the ozone flux from the stomata into the vegetation that exceeds the threshold.

$$F = 1 - a \cdot \max[(F_{ozn} - F_{ozncrit}), 0], \qquad (7)$$

where a is the sensitivity parameter of vegetation to ozone obtained based on observation data. $F_{ozncrit}$ represents the threshold corresponding to the damage caused by ozone to vegetation, $F_{ozn}$ represents the flux of ozone entering the page through the stomata:

$$F_{ozn} = \frac{[O_3]}{r_b + \frac{\kappa_{O3}}{r_s}}, \qquad (8)$$

where $[O_3]$ is the ozone concentration at the top of the canopy, $r_b$ is the boundary layer resistance, $\kappa_{O3}$ is the ratio of $O_3$ leaf resistance to water vapor blade resistance, $r_s$ is the stomatal resistance considering the influence of ozone:

$$r_s = g_s \cdot F. \qquad (9)$$

$g_s$ is the leaf conductance without $O_3$ effects. The set of equations (7), (8) and (9) yields a quadratic term in F

242     that can be solved analytically.

**2.4 Descriptions of the RegCM-Chem-YIBs model**

**2.4.1 Coupling between RegCM-Chem and YIBs**

245        The integrated RegCM-Chem-YIBs model, an enhancement to the original RegCM-Chem, introduces $CO_2$

246     as an atmospheric constituent, incorporating its source-sink dynamics, transport, and diffusion processes. At-

247     mospheric $CO_2$ concentration is primarily influenced by atmosphere-ocean $CO_2$ exchange flux, biomass com-

248     bustion emissions, fossil fuel emissions, and terrestrial ecosystem $CO_2$ flux. The model prescribes fossil fuel

249     emissions, biomass combustion emissions, and atmosphere-ocean $CO_2$ fluxes, while the terrestrial ecosystem

250     $CO_2$ fluxes are computed in real time via the coupled YIBs terrestrial ecosystem model.

251        Within the coupled model system, meteorological variables (including temperature, humidity, precipitation,

252     radiation, etc.) and atmospheric pollutant concentrations ($O_3$ and $PM_{2.5}$) generated by RegCM-Chem are incor-

253     porated into the YIBs model every six-minute intervals. This integration step is to be consistent with the integra-

254     tion time step of the chemistry module, thus maintaining synchronization between modules. Considering the

255     complexity of chemical reactions and ecological processes, dynamic adjustments at short intervals enable the

256     model to better capture transient interactions between ecology and the atmosphere. The choice of this adjust-

257     ment frequency balances the representation of actual processes with computational efficiency, ensuring that

258     simulation results are both accurate and efficient. YIBs then simulates vegetation physiological processes such

259     as photosynthesis and respiration, computing land surface parameters including $CO_2$ flux, BVOC, and stomatal

260     conductance. These outputs from the YIBs are subsequently integrated back into the RegCM-Chem model every

261     six-minute intervals, the intricacies of this integration process lead to significant changes in various environ-

262     mental parameters. The major direct changes, prominently influencing the model's behavior, arise from altera-

263     tions in $CO_2$ concentration. These changes are directly attributed to intricate physiological processes within the

264     vegetation, including photosynthesis and respiration. The fluxes of $CO_2$ through these biological processes play

265     a pivotal role in shaping the atmospheric composition. On the indirect front, the integration of YIBs outputs in-

266     duces intricate variations in $PM_{2.5}$ and $O_3$ concentrations. These indirect changes are primarily orchestrated by

267     shifts in BVOC emissions. The dynamic nature of these emissions contributes to the complexity of atmospheric

268     chemistry, influencing the levels of $PM_{2.5}$ and $O_3$. Simultaneously, the integration process plays a crucial role in

269     shaping the temporal variations of atmospheric temperature, humidity, and circulation. These changes over time

are intricately linked to variations in land surface parameters. The interplay of these variables illustrates the dynamic feedback loops between climate, chemical composition, and ecological processes within the integrated model system.

**2.4.2 Model input data**

The input data of RegCM-Chem-YIBs mainly includes four categories: surface data, initial boundary data, anthropogenic emission data and $CO_2$ surface flux data, which are detailed below.

(1) Surface data include surface vegetation cover type, terrain, and leaf area index. Land cover type information is obtained from the MODIS and AVHRR satellites, employing the classification scheme suggested by Lawrence and Chase (Lawrence and Chase, 2007), which uses MODIS data to preliminarily distinguish forest, grassland, bare soil, etc., and combine this with AVHRR data to make a detailed forest classification. The dataset contains a total of 16 different vegetation functional types. To align with the classification conventions of the YIBs model, the original 16 vegetation functional types were converted into the corresponding 8 types recognized by the YIBs model. The results are shown in Figure S1.

(2) Initial and boundary data include initial and boundary conditions of meteorological variables and atmospheric chemical composition. Here we use ERA-Interim reanalysis meteorological data, a product from the European Center for Medium-Range Weather Forecasts (ECMWF) created through four-dimensional variational assimilation. The data is on 37 vertical levels, with a horizontal resolution of 0.125°×0.125°, and time resolution of 6 hours. Data for Sea Surface Temperature (SST) is provided by the weekly averaged Optimum Interpolation SST product (OI_WK) of the National Oceanic and Atmospheric Administration (NOAA) (Reynolds et al., 2002). The initial and boundary conditions of atmospheric chemical components (e.g. $O_3$), come from simulations carried out with the global chemistry model MOZART (Emmons et al., 2010; Horowitz et al., 2003). In addition, the initial and boundary conditions for $CO_2$ species come from the CarbonTracker global carbon assimilation system (Peters et al., 2007) developed by NOAA Earth System Research Laboratory ESRL (Earth System Research Laboratory), which uses the ensemble Kalman filter algorithm to assimilate ESRL greenhouse gas observations and $CO_2$ observation data provided by the network of collaborating institutions worldwide. The assimilated data includes not only conventional fixed-site observations but also mobile monitoring data such as aircraft and ships. Since 2007, yearly updated carbon assimilation products are provided by CarbonTracker, delivering global $CO_2$ three-dimensional concentration data products every three hours. In this study, we utilized

the CT2019 product, updated in 2019, spanning a period from January 1, 2000 to March 29, 2019.

(3) Anthropogenic emission data include precursors of ozone and particulate matter such as NOx, VOC, BC, OC, etc. The MIX Asian anthropogenic emission inventory developed by the Tsinghua University is used (Li et al., 2017b), which integrates the results of the emission inventories of various regions in Asia. The emissions in China come from China's multi-scale emission inventory MEIC (Multi-resolution Emission Inventory for China) and the high-resolution $NH_3$ emission inventory developed by Peking University. The anthropogenic emissions in India come from the Indian local emission inventory developed by ANL (Argonne National Laboratory), while the anthropogenic emissions in South Korea come from the CAPSS (The Korean local emission inventory developed by the Policy Support System), and the man-made emissions in other regions are provided by the REAS (Regional Emission inventory in Asia) emission inventory version 2.1. The anthropogenic emissions of major pollutants in the simulated area are shown in Figure S2.

(4) Data pertaining to fossil fuel $CO_2$ emissions are sourced from the MIX Asian anthropogenic emission inventory with a monthly time resolution. $CO_2$ emissions resulting from biomass burning are derived from the FINN (Fire Inventory from NCAR) inventory (Wiedinmyer et al., 2011) developed by the National Center for Atmospheric Research. The FINN inventory has a daily time resolution. The model's ocean-atmosphere $CO_2$ exchange flux is obtained from the carbon flux product of the CarbonTracker assimilation system, constructed with the global atmospheric transport model TM5 and assimilating $CO_2$ observation data via an ensemble Kalman filter algorithm. This provides global $1°\times1°$ resolution $CO_2$ exchange flux data between the ocean and the atmosphere updated every three hours. The emissions are detailed in Figure S3.

**3 Model Application**

**3.1 Model setup**

To evaluate the performance of RegCM-Chem-YIBs we carried out a one-year simulation starting from December 1st, 2015, through December 31st, 2016. The initial month is used as spin-up period, and thus it is not included in the analysis. The simulation domain is centered at 36°N, 107°E, and covers a considerable part of East Asia, including China, Japan, the Korean Peninsula, and Mongolia, along with significant parts of India and Southeast Asia (Figure S4). The horizontal grid spacing is 30 km and we use 14 levels in the vertical, reaching up to 50 hPa. Section 2.4.2 provides a comprehensive description of the model input data.

**3.2 Climate simulations in East Asian**

326     Given the importance of the climate for the East Asia region, we first present an assessment of the simula-

327 tion for the climate 2016 by comparison with the ERA-Interim data. The simulated temperature, specific

328 humidity, and wind fields at varying altitudes and seasons compared well with the reanalyzed data (Figure S5~

329 Figure S9), especially temperature and specific humidity, while a tendency to overestimate wind speed is

330 observed at the near surface and 850 hPa levels. The fields at 500 hPa show very close agreement with

331 reanalysis data, indicating a strong mid-atmosphere forcing by the boundary conditions, while the simulated

332 circulation patterns near the surface and at 850 hPa in summer tend to deviate more from the driving reanalysis.

333 The simulated circulation patterns in the other seasons are basically consistent with the reanalysis data.

334     We first calculated the daily average of the meteorological variables, such as temperature, wind speed, and

335 specific humidity, from the model simulation and reanalysis data, respectively. Then we calculate the

336 corresponding statistical indicator correlation coefficient (R), mean deviation (MB), and root mean square error

337 (RMSE) based on the daily averages. Table 1 reports a number of statistical metrics of comparison between

338 simulated and reanalysis meteorological variables at different heights. Correlation coefficients (R) range from

339 0.95 to 0.98 for temperature, 0.71 to 0.97 for longitudinal wind, 0.81 to 0.92 for latitudinal wind, and 0.91-0.92

340 for specific humidity, indicating a general good consistency between model and driving data, in line with previ-

341 ous studies (Zhuang et al., 2018; Zhou et al., 2014; Wang et al., 2010).

342 **Table 1.** Statistical indicators for comparison between model simulation results and reanalysis data

| Heights | Statistical index | Air Temperature(K) | Longitudinal wind (m/s) | Latitudinal wind (m/s) | Specific humidity (kg kg$^{-1}$) |
|---|---|---|---|---|---|
| 500 hpa | R | 0.98 | 0.97 | 0.92 | 0.91 |
| | MB | 0.15 | 0.35 | -0.03 | 0.00015 |
| | RMSE | 0.93 | 0.75 | 0.51 | 0.00019 |
| 850 hpa | R | 0.96 | 0.77 | 0.85 | 0.94 |
| | MB | -0.98 | 0.38 | 0.15 | -0.00066 |
| | RMSE | 1.1 | 1.08 | 0.59 | 0.00077 |
| Near surface | R | 0.95 | 0.71 | 0.81 | 0.92 |
| | MB | -1.21 | 0.33 | 0.23 | -0.00098 |
| | RMSE | 1.35 | 0.59 | 0.54 | 0.00112 |

(Correlation coefficients (R), mean biases (MB), and root mean square error (RMSE))

The magnitude of surface radiation flux directly determines the rates of photosynthesis in vegetation. For verification purposes, model surface solar fluxes were compared with data on solar energy at the surface retrieved from the Clouds and the Earth's Radiant Energy System (CERES) satellite, which has a $1° \times 1°$ horizontal and monthly temporal resolution. Figure S10 shows the simulated surface net shortwave radiation in different seasons and comparison with observational data. The model tends to overestimate surface net shortwave radiation in spring and winter over India and summer over North China (Yin et al., 2014). Overall, the simulated surface net shortwave radiation agrees well with the CERES satellite retrieval results, capturing the spatial distribution and seasonal fluctuation patterns of surface shortwave radiation. The simulation findings from our study are consistent with earlier research regarding surface net shortwave radiation (Han et al., 2016).

In conclusion, RegCM-Chem-YIBs demonstrates a good performance in simulating the climatological features of the East Asia atmospheric circulations, effectively reproducing the spatial distribution and seasonal variations of temperature, specific humidity, and radiation.

**3.3 Simulations of** $PM_{2.5}$**,** $O_3$ **and** $CO_2$

In this section, we compare simulated $PM_{2.5}$ and $O_3$ concentrations against observational data from 366 stations provided by the China National Environmental Monitoring Center. The geographical distribution of the simulated annual mean near-surface daily $PM_{2.5}$ and maximum daily 8-hour average (MDA8) $O_3$ concentration, along with the observed values, are shown in Figure 2. Supplementary Figure S11 then compares in a scatter-plot format the observation and simulation results. Both figures demonstrate that the model reproduces the spatial distribution patterns of $PM_{2.5}$ and $O_3$, with a significant agreement between modeled and measured values across all stations. The statistical indicators of simulated and measured surface $PM_{2.5}$ and $O_3$ levels are shown in Table S1, showing a correlation between simulation and observations of $O_3$ and $PM_{2.5}$ of 0.74 and 0.65, respectively. The simulated $O_3$ concentrations are generally lower than observed in the Fenwei Plain of China, a discrepancy possibly attributable to uncertainties in the emission inventory for this region. In summary, the RegCM-Chem-YIBs model demonstrates a good ability to capture the spatial distribution of observed near-surface ozone and particulate matter, especially in highly polluted areas.
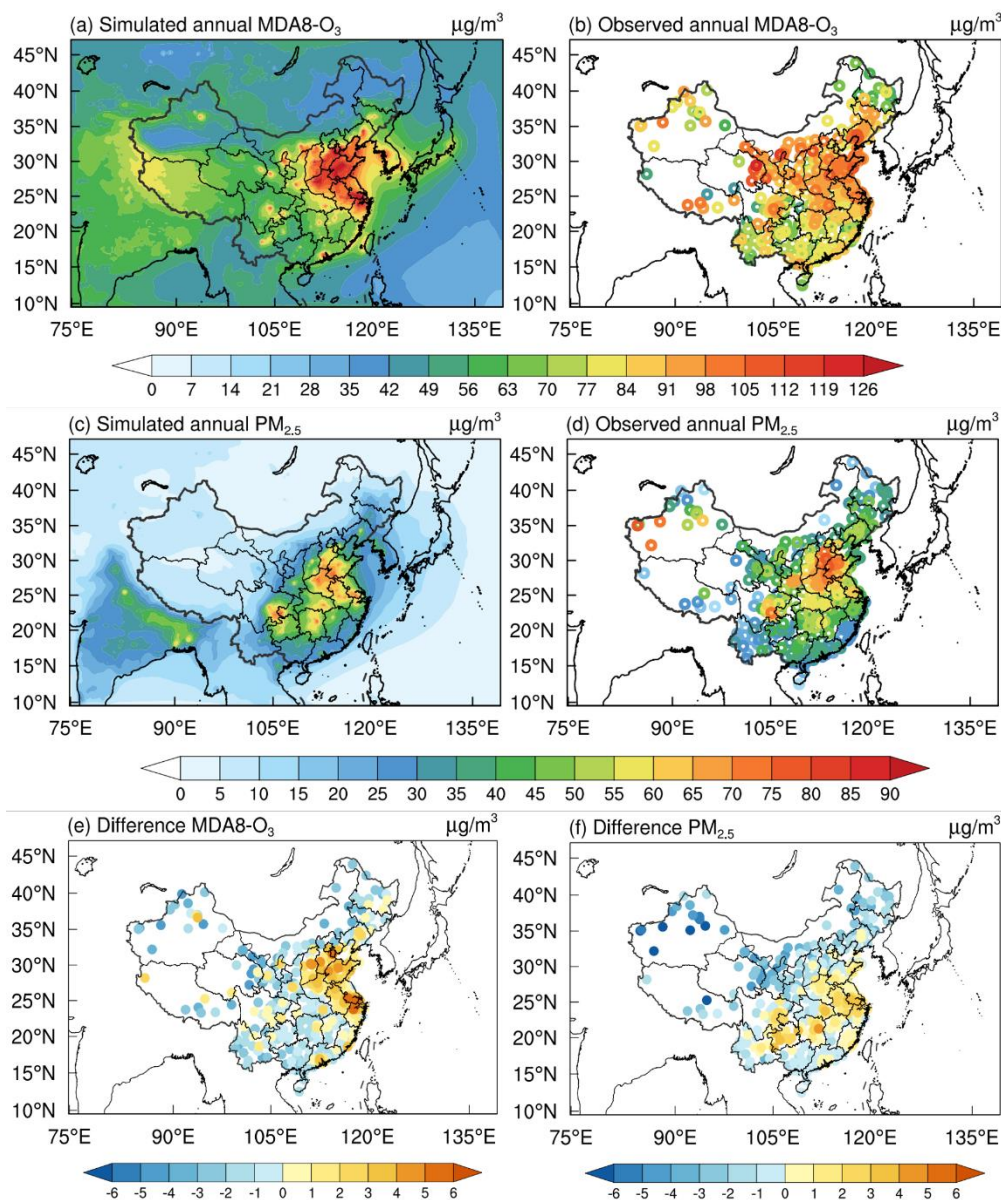
**Figure 2.** Simulation and observation comparison of (a, b) $O_3$ and (c, d) $PM_{2.5}$ and their differences (e, f) in China. The differences are simulation minus observation. The colored circles in the figure represent station observations. Units: $\mu g\ m^{-3}$.

Measured and calculated monthly mean $CO_2$ concentrations at six observation stations in East Asia from the World data Center for Greenhouse Gases are shown in Figure 3. Information on the six sites is listed in Table 2. The simulated $CO_2$ concentration agrees well with observations, with correlation coefficients ranging from 0.89 to 0.97. However, in urban and coastal areas, the model performance deteriorates likely due to local emission fluctuations and errors in biogenic fluxes. Nevertheless, the model overall captures the seasonal variations in $CO_2$ concentrations (Figure 3). This result likely stems from the complex relationship between biogenic and fossil fuel emissions, which are known contributors to observed seasonal $CO_2$ patterns (Kou et al., 2015). A high

CO$_2$ mixing ratio (412.3 ppm) is observed at the TAP site, which is associated with strong local emissions. Further analysis into the specific sources contributing to elevated CO$_2$ levels would provide valuable insights into localized patterns of emissions and their effects on regional carbon cycle processes. The model's ability to reproduce the geographical and seasonal CO$_2$ patterns serves as an illustration of its ability to capture the main processes driving CO$_2$ dynamics. In summary, while discrepancies in urban or coastal areas highlight the challenges associated with capturing localized CO$_2$ dynamics, the model's overall performance and ability to reproduce geographical and seasonal CO$_2$ patterns demonstrates its usefulness in studying CO$_2$ dynamics at a regional scale.

**Table 2.** Information on six CO$_2$ stations in East Asia and statistical indicators of observed and modeled CO$_2$.

| Sites | Latitude | Longitude | Elevation | Observations (ppm) | Simulations (ppm) | R | RMSE |
|-------|----------|-----------|-----------|--------------------|--------------------|------|------|
| WLG | 36.29 | 100.90 | 3810 | 404.3 | 402.9 | 0.94 | 1.75 |
| TAP | 36.72 | 126.12 | 20 | 412.3 | 414.8 | 0.97 | 2.70 |
| UUM | 44.45 | 111.08 | 992 | 405.7 | 403.7 | 0.96 | 2.66 |
| LLN | 23.46 | 120.86 | 2867 | 406.0 | 407.2 | 0.93 | 1.63 |
| YON | 24.47 | 123.02 | 30 | 407.1 | 407.4 | 0.89 | 2.80 |
| HK | 22.31 | 114.17 | 65 | 407.9 | 409.7 | 0.92 | 15.67 |

(Correlation coefficients (R) and root mean square error (RMSE))
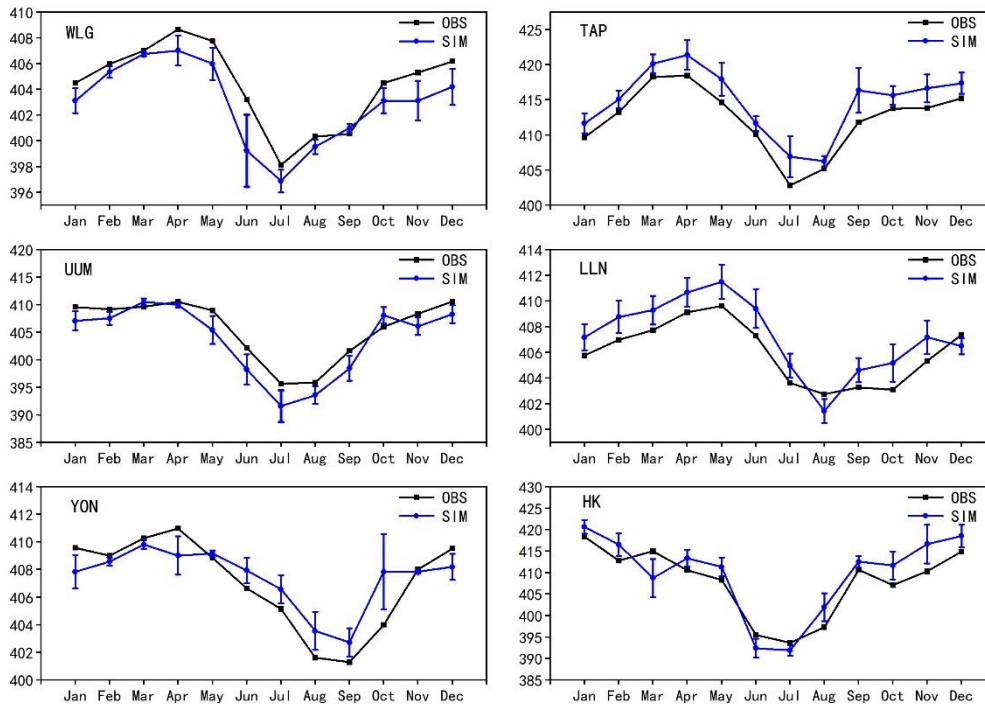
**Figure 3.** Modeled (blue) and observed (black) monthly mean $CO_2$ concentrations validated at six sites in East Asia. Units: ppm.

The limitations of ground-based $CO_2$ observation stations, particularly their sparse spatial distribution, pose challenges in obtaining high-resolution $CO_2$ data. To offset this limitation, data assimilation methods have been implemented to ensure a coherent global distribution of atmospheric $CO_2$, effectively filling the void left by sparse ground-based observations. Here we utilize the Carbon Tracker global carbon assimilation system developed by the NOAA Earth System Research Laboratory (ESRL) to validate the simulated $CO_2$ concentrations (Peters et al., 2007). This comparison for the year 2016 is shown in Figure 4. The simulated $CO_2$ concentrations tend to be lower than observed in Northeastern India and Northeastern China, while they show a better agreement with observations in other regions. These discrepancies can be traced back to factors such as the underestimation of localized $CO_2$ emissions along with the effects of complex topography and circulation patterns. However, the closer agreement in other regions suggests that the model effectively captures the primary processes driving $CO_2$ concentrations.

Seasonal variations in the spatial distribution of $CO_2$ concentrations for 2016 are illustrated in supplementary Figure S12. The simulations show marked seasonal variations, with elevated concentrations in spring, autumn, and lower values during summer. In northern regions, including Russia, Mongolia, and Northeast China, the lowest near-surface $CO_2$ concentrations occur in summer. This pattern can be attributed to the enhanced

17

photosynthetic activity of terrestrial vegetation in summer, leading to enhanced atmospheric $CO_2$ sequestration. Conversely, winter months are characterized by lower solar radiation fluxes and reduced vegetation photosynthesis, resulting in relatively higher $CO_2$ concentrations. In specific regions, notably the eastern coastal zones of China and South Korea, the seasonal pattern of $CO_2$ concentration is reduced, likely because of the high levels of urbanization, dense population, and intense anthropogenic emissions in these areas. In contrast, regions such as Yunnan, the southern side of the Qinghai-Tibet Plateau, and Southeast Asia exhibit consistently low $CO_2$ concentrations during summer because of significant vegetation sinks in these densely vegetated areas. An increase in $CO_2$ concentrations can be observed over these regions during spring due to local forest fires and straw-burning processes, which release substantial amounts of $CO_2$ into the atmosphere (Chuang et al., 2014).
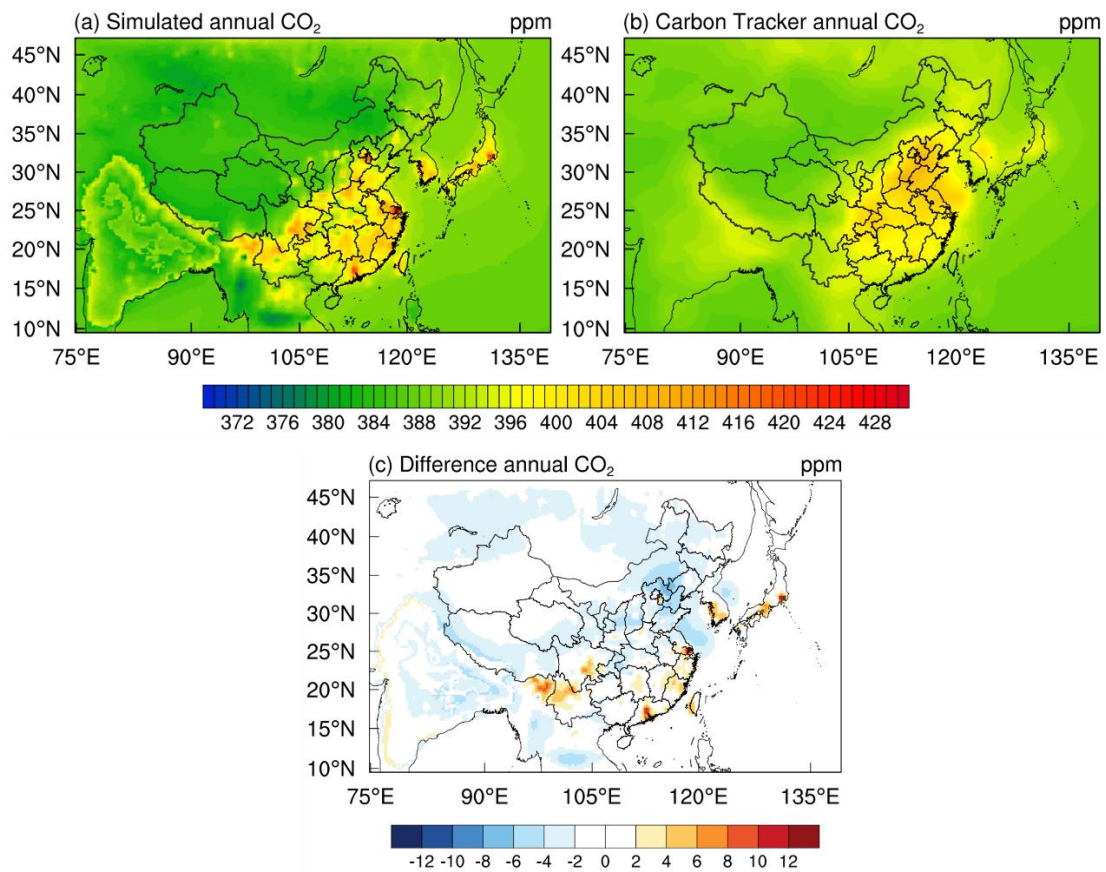


**Figure 4.** Evaluation of simulated $CO_2$ (a) using Carbon Tracker products (b) and their difference (c) in 2016. The differences are simulation minus observation. Units: ppm.

### 3.4 Simulations of carbon fluxes in terrestrial systems

Our assessment of GPP and NPP uses the MOD17A3 Collection 6, a global product originating from MODIS satellite observations. GPP data include 8-day values with a resolution of 500 meters, as produced in

423   MOD17A2H Version 6 based on radiation use efficiency theory. Such data can be used as input to computations

424   of terrestrial carbon and energy flows, water cycling processes, and vegetation biogeochemistry. Moreover, the

425   MOD17A3H Version 6 product provides information on annual NPP, also on a resolution of 500 meters. All

426   8-day Net Photosynthesis (PSN) products (MOD17A2H) from a particular year are combined to derive annual

427   NPP values (He et al., 2018; Madani et al., 2014; Running, 2012).

428   Figure 5 (a, b, e) shows the geographical distribution of the mean GPP in 2016 from the model simulations

429   and MODIS products. RegCM-Chem-YIBs effectively captures the observed spatial GPP features, with high

430   values mostly over Southwest, Central, and Southeastern China, areas characterized by deciduous broad-leaf

431   and evergreen coniferous forests (Figure S1). The annual average GPP simulated by RegCM-Chem-YIBs is

432   higher than observed over   Southwest and Central China by 6.8% and 12.7%, respectively. The annual average

433   simulated GPP over China is 6.18 Pg C $yr^{-1}$, which is about 7.56% higher than the GPP in MODIS.

434   Figure 6 (a) and Table S2 show the scatter plots of the simulated annual average GPP on each model grid

435   point compared with MODIS. A correlation coefficient of 0.91 and root mean square error of 0.4 kg C $m^{-2}$ $yr^{-1}$ is

436   found,   reflecting an overall good simulation by the model. Compared with the results obtained from the global

437   model NASA ModelE2–YIBs (Yue and Unger, 2017), the GPP value estimated here compares better with the

438   MODIS product, which may also be attributed to the higher spatial resolution of the regional system. Moreover,

439   our GPP results are also in line with earlier findings, such as from Li (Li et al., 2013b) who estimated an annual

440   average GPP over China of 6.04 Pg C $yr^{-1}$ based on the light energy utilization model EC-LUE.

441   Figure 5 (c, d, f) shows the spatial distribution of mean NPP for both the simulations and MODIS

442   products in 2016. NPP, similarly to GPP, exhibits a gradual reduction from southeast to northwest China. The

443   scatter plot comparing the simulated and MODIS annual average NPP across the model grid is illustrated in

444   Figure 6 (b). According to Table S2, a correlation coefficient of 0.87 is found between the simulated and

445   MODIS NPP, with a root mean square error of 0.22 kg C $m^{-2}$ $yr^{-1}$. Notably, the simulated NPP shows a distinct

446   underestimation over regions with higher NPP values. Compared with the MODIS NPP data products, the

447   annual average NPP simulated for the entire China region in 2016 is overestimated by approximately 8.64%,

448   mostly because of the model overestimate in Central China (16.6%).

449   Part of the reason for this result is the relatively simple treatment of the nitrogen deposition process in YIBs

450   (Yue and Unger, 2015). On the other hand, some studies have noted that due to the limitations of driving data

451   and algorithm parameters, the MODIS NPP products have some problems in China (Li et al., 2013b).

452    Furthermore, the NPP value estimated by the model over China is 3.21 Pg C yr$^{-1}$, in line with the mean value

453    (2.92 ± 0.12 Pg C yr$^{-1}$) found in previous 37 studies (Wang et al., 2017).
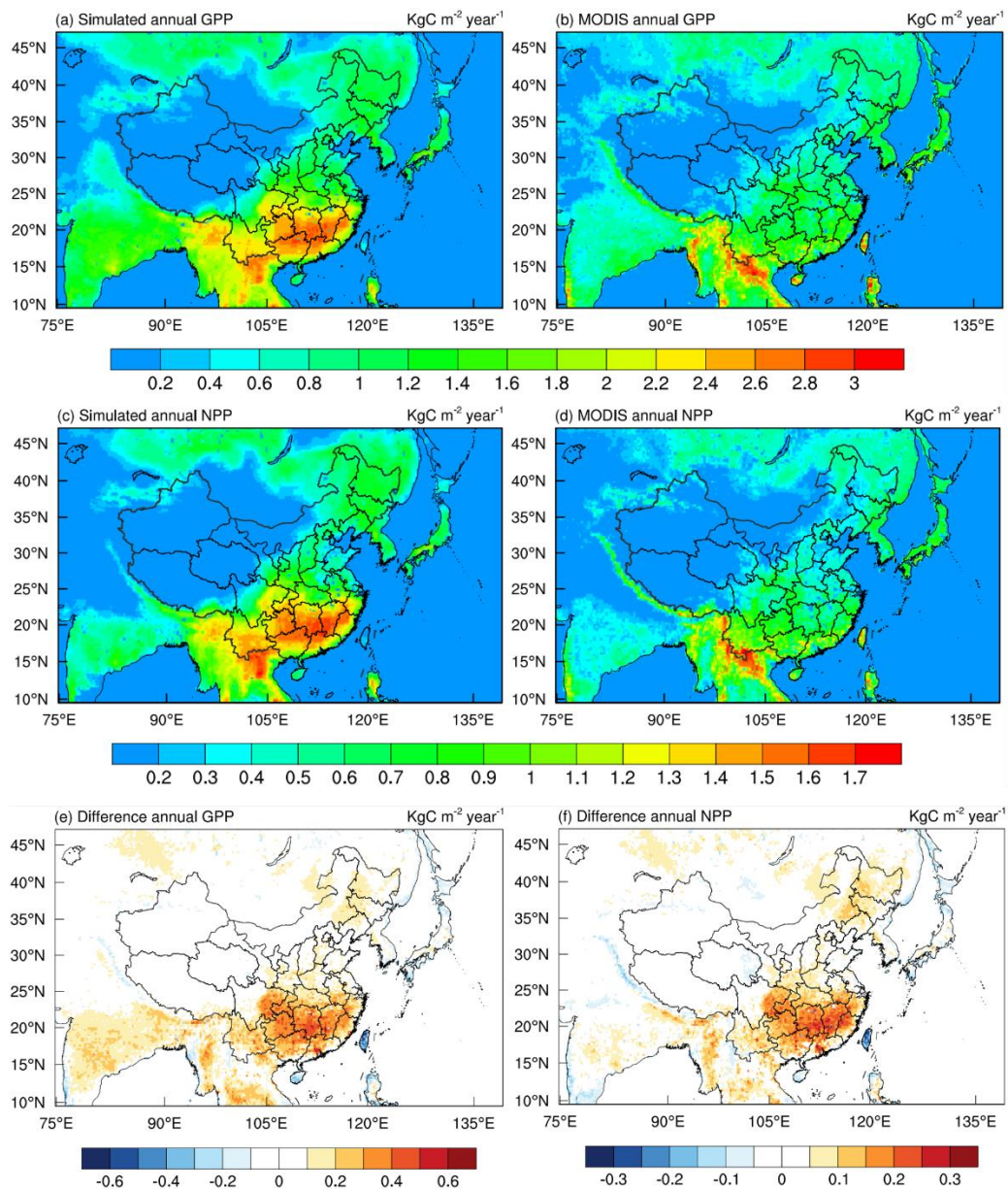
454



455    **Figure 5.** Spatial distribution of modeled (a, c) and MODIS (b, d), annual mean GPP (a, b) and NPP (c, d), and

456    their differences (e, f). The differences are simulation minus observation. Units: kg C m$^{-2}$ year$^{-1}$.

457
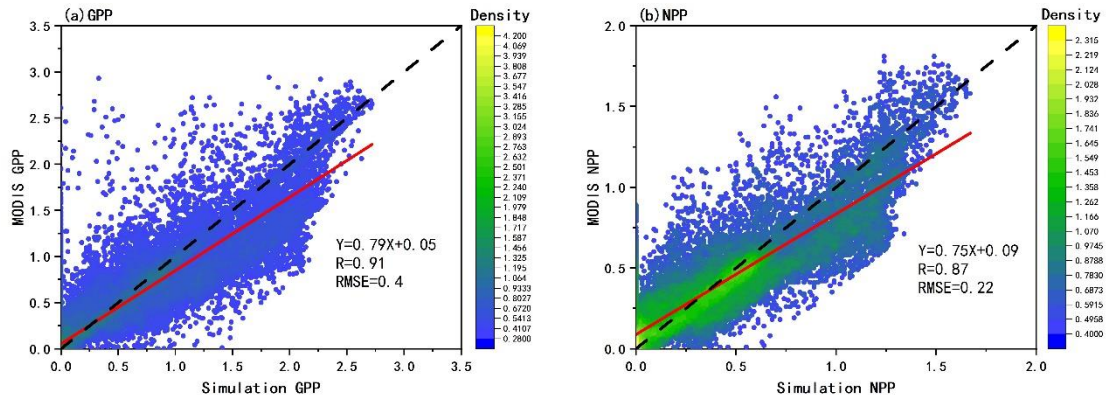
**Figure 6.** Density scatter plots of (a) GPP and (b) NPP for model simulations and inversion-based products for 2016. Units: kg C m$^{-2}$ year$^{-1}$.

Figure 7 and Figure 8 illustrate the seasonal fluctuations in GPP and NPP, as simulated for 2016 in East Asia. Both GPP and NPP present pronounced seasonal variations, with negligible values during winter, and a strong peak in summer. The winter minimum is attributable to limiting environmental factors such as reduced solar radiation, lower temperatures, and suppressed photosynthetic activity by vegetation. Conversely, summer shows the highest GPP and NPP values due to extended daylight hours, increased solar radiation, and temperatures facilitating increased photosynthetic activity and vegetation metabolism.



466
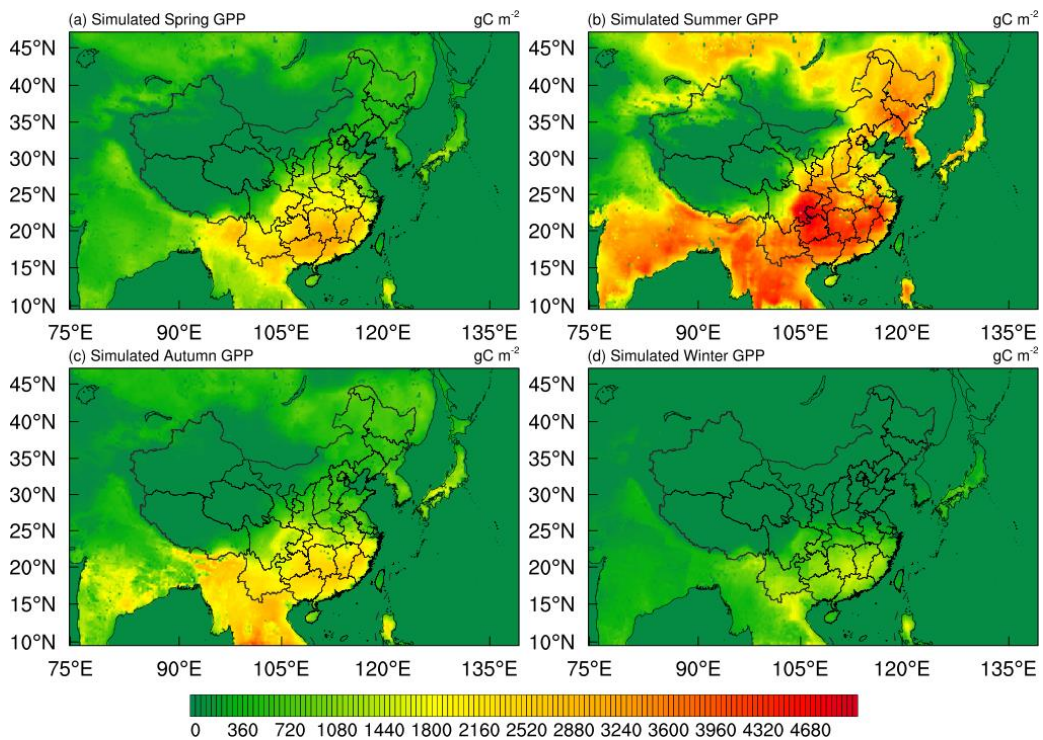
**Figure 7.** Spatial distribution of GPP simulated by model of spring(a), summer(b), autumn(c) and winter(d) in 2016. Units: g C m$^{-2}$
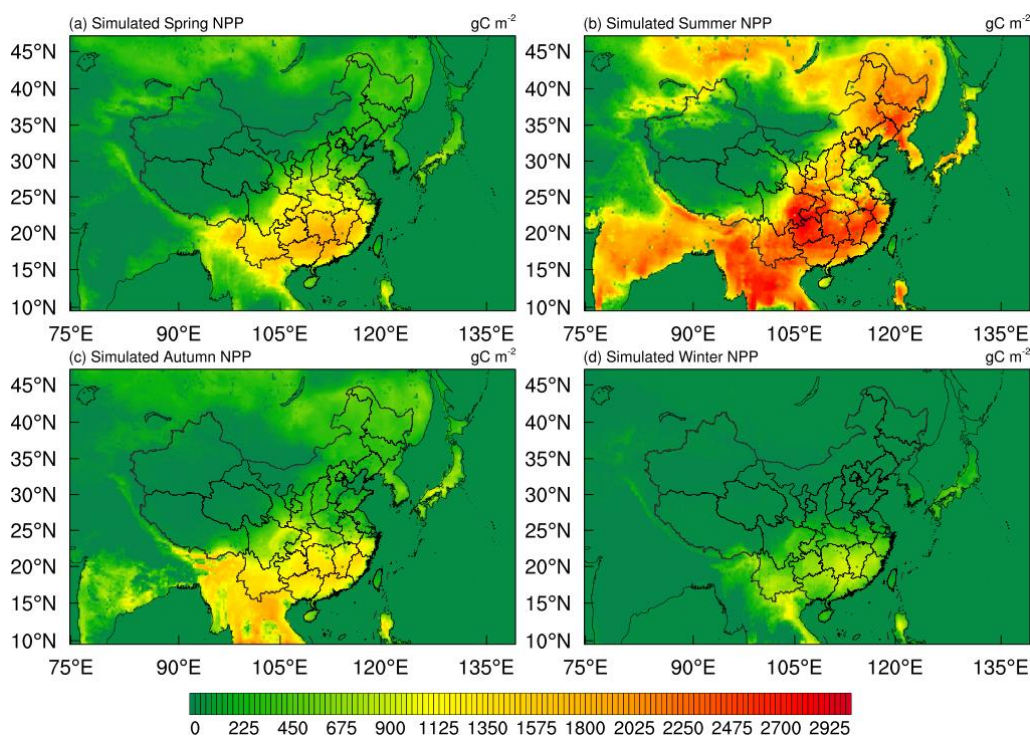
**Figure 8.** Spatial distribution of NPP simulated by model of spring(a), summer(b), autumn(c) and winter(d) in 2016. Units: g C m$^{-2}$

**3.5 Simulations of other carbon-bearing species**

The analysis of additional carbonaceous compounds such as BC, OC and carbon monoxide (CO), is crucial due to their considerable influence on climate and the carbon cycle. The spatial distribution of simulated BC for each season of 2016 is shown in Figure S13. BC concentrations are mainly centered in North China, Central China, the Sichuan Basin, Chongqing, and Northeast India, regions with a higher concentration of industrial and residential emission sources. BC displays a marked seasonal variation, with elevated levels in winter, possibly attributed to residential heating, more stagnant conditions, and reduced removal by precipitation.

Figure S14 then shows the spatial corresponding distribution of seasonal OC, which is also higher over North China, Central China, Sichuan and Chongqing, and Northeast India. Finally, Figure S15 reports the annual mean near-surface CO concentrations for observations and simulation data across the monitoring sites in China. While simulated CO concentrations agree well spatially with observations, the simulations produce higher values than observed in Central China, likely linked to uncertainties in emission inventories. Figure S16 presents the seasonal spatial distributions of CO, with simulated high values mostly localized in Sichuan-Chongqing and Central China, and a peak in winter.

## 4 Conclusions

Regional climate-chemical coupled models can be used to study the characteristics of regional-scale climate and pollutants, and is an important means to investigate the behavior of atmospheric pollutants and their radiative climate effects. However, current coupled regional climate models describe the physiological process of terrestrial vegetation relatively simply and do not consider the interaction between atmospheric pollutants (such as $PM_{2.5}$ and $O_3$) and $CO_2$, as well as their impacts on terrestrial ecosystems.

To overcome this problem, in this work we coupled the YIBs biogeochemical model to the RegCM-CHEM regional climate-chemistry model, and tested this coupled modeling system over a domain covering East Asia at a 30 km horizontal grid spacing for the year 2016. The model output was validated against reanalysis data, observational data, and satellite remote sensing data, both for the atmosphere and the carbon cycle.

Our simulations show that the coupled RegCM-Chem-YIBs system can effectively reproduce the spatio-temporal distribution of meteorological variables, atmospheric composition ($PM_{2.5}$, $O_3$, and $CO_2$) and terrestrial carbon fluxes (GPP and NPP). Comparisons of the simulated temperature, longitudinal wind, latitudinal wind, and specific humidity for different seasons with the driving ERA-Interim reanalysis data showed correlation coefficients of 0.95-0.98, 0.71-0.97, 0.81-0.92, and 0.91-0.92, respectively. The correlation coefficients between observed and simulated $O_3$ and $PM_{2.5}$ levels in China were 0.74 and 0.65, respectively, while the corresponding correlations for $CO_2$ were in the range of 0.89 to 0.97. Comparison of the ecological parameters GPP and NPP simulated in East Asia with the observed data showed correlation coefficients of 0.91 and 0.87, respectively. In addition, in all cases, the seasonal variation of the different variables was captured by the model. Therefore, we conclude that, overall, the RegCM-Chem-YIBs model demonstrates a good performance in simulating the spatio-temporal distribution characteristics of regional meteorological characteristics, atmospheric composition, and ecological parameters over East Asia.

In the future, we will continue to improve RegCM-Chem-YIBs in the following aspects. First, we will investigate the impact of $CO_2$ and $O_3$ inhomogeneity on radiation calculations by integrating temporally and spatially varying concentrations derived from YIBs and Chem into the RegCM radiation module. This will enable additional accurate computation of longwave radiation flux, improving the representation of the regional radiation balance. Second, we intend to assimilate a module representing various chemical transformations happening on the surfaces of aerosol particles. Finally, we will include the wet removal process of $O_3$. These advancements will contribute to the refinement of RegCM-Chem-YIBs, enhancing our ability to investigate the interactions

515     between regional atmosphere, carbon cycle, and vegetation processes.

**Code and data availability**

517     The RegCM-Chem source code can be obtained from https://github.com/ICTP/RegCM (last access: 10 July
518     2023). The YIBs model code is available at https://github.com/YIBS01/YIBs_site (last access: 10 July 2023).
519     The input data and source code for RegCM-Chem-YIBs have been archived on Zenodo at
520     https://doi.org/10.5281/zenodo.8186164 (Xie and Wang, 2023). The CarbonTracker data are provided at
521     (https://gml.noaa.gov/ccgg/carbontracker/). The CERES surface radiation data are available at
522     (https://ceres.larc.nasa.gov/). WDCGG data are available at (https://gaw.kishou.go.jp/). CNEMC data are pro-
523     vided at (http://www.cnemc.cn/). MODIS data are available at (https://ladsweb.modaps.eosdis.nasa.gov/).

**Author contributions**

525     TW led the development of RegCM-Chem-YIBs with significant contributions from NX and XX. NX per-
526     formed the evaluation. NX, TW drafted the manuscript and all authors contributed to review and editing of the
527     manuscript.

**Competing interests**

529     The corresponding author has stated that all the authors have no conflicts of interest.

**Disclaimer**

531     Publisher's note: Copernicus Publications remains neutral about jurisdictional claims in published maps and
532     institutional affiliations.

**Acknowledgments**

**References**

Ahlstrom, A., Raupach, M. R., Schurgers, G., Smith, B., Arneth, A., Jung, M., Reichstein, M., Canadell, J. G., *et al.*: The dominant role of semi-arid ecosystems in the trend and variability of the land CO2 sink, Science, 348, 895-899, https://doi.org/10.1126/science.aaa1668, 2015.

Ainsworth, E. A., Yendrek, C. R., Sitch, S., Collins, W. J., and Emberson, L. D.: The Effects of Tropospheric Ozone on Net Primary Productivity and Implications for Climate Change, Annu. Rev. Plant Biol., 63, 637-661, https://doi.org/10.1146/annurev-arplant-042110-103829, 2012.

Artale, V., Calmanti, S., Carillo, A., Dell'Aquila, A., Herrmann, M., Pisacane, G., Ruti, P. M., Sannino, G., *et al.*: An atmosphere-ocean regional climate model for the Mediterranean area: assessment of a present climate simulation, Clim. Dyn., 35, 721-740, https://doi.org/10.1007/s00382-009-0691-8, 2010.

Baklanov, A., Molina, L. T., and Gauss, M.: Megacities, air quality and climate, Atmos. Environ., 126, 235-249, https://doi.org/10.1016/j.atmosenv.2015.11.059, 2016.

Chang, J. S., Brost, R. A., Isaksen, I. S. A., Madronich, S., Middleton, P., Stockwell, W. R., and Walcek, C. J.: A 3-DIMENSIONAL EULERIAN ACID DEPOSITION MODEL - PHYSICAL CONCEPTS AND FORMULATION, J. Geophys. Res.: Atmos., 92, 14681-14700, https://doi.org/10.1029/JD092iD12p14681, 1987.

Chuang, M. T., Lee, C. T., Chou, C. C. K., Lin, N. H., Sheu, G. R., Wang, J. L., Chang, S. C., Wang, S. H., *et al.*: Carbonaceous aerosols in the air masses transported from Indochina to Taiwan: Long-term observation at Mt. Lulin, Atmos. Environ., 89, 507-516, https://doi.org/10.1016/j.atmosenv.2013.11.066, 2014.

Chutia, L., Ojha, N., Girach, I. A., Sahu, L. K., Alvarado, L. M. A., Burrows, J. P., Pathak, B., and Bhuyan, P. K.: Distribution of volatile organic compounds over Indian subcontinent during winter: WRF-chem simulation versus observations, Environ. Pollut., 252, 256-269, https://doi.org/10.1016/j.envpol.2019.05.097, 2019.

Collatz, G. J., Ball, J. T., Grivet, C., and Berry, J. A.: Physio-logical and Environmental-Regulation of Stomatal Conductance, Photosynthesis and Transpiration – a Model That Includes a Laminar Boundary-Layer, Agric. For. Meteorol., 54, 107-136, https://doi.org/10.1016/0168-1923(91)90002-8, 1991.

Coppola, E., Poulton, M., Charles, E., Dustman, J., and Szidarovszky, F.: Application of Artificial Neural Networks to Complex Groundwater Management Problems, Nat. Resour. Res., 12, 303-320, https://doi.org/10.1023/B:NARR.0000007808.11860.7e, 2003.

Dickinson, R. E., Errico, R. M., Giorgi, F., and Bates, G. T.: A Regional Climate Model for the Western United-States, Clim. Change, 15, 383-422, https://doi.org/10.1007/BF00240465, 1989.

Dunne, J. P., Horowitz, L. W., Adcroft, A. J., Ginoux, P., Held, I. M., John, J. G., Krasting, J. P., Malyshev, S., *et al.*: The GFDL Earth System Model Version 4.1 (GFDL-ESM 4.1): Overall Coupled Model Description and Simulation Characteristics, J. Adv. Model. Earth Syst., 12, https://doi.org/ARTNe2019MS00201510.1029/2019MS002015, 2020.

Emmons, L. K., Walters, S., Hess, P. G., Lamarque, J. F., Pfister, G. G., Fillmore, D., Granier, C., Guenther, A., *et al.*: Description and evaluation of the Model for Ozone and Related chemical Tracers, version 4 (MOZART-4), Geosci. Model Dev., 3, 43-67, https://doi.org/10.5194/gmd-3-43-2010, 2010.

Farquhar, G. D., Caemmerer, S. V., and Berry, J. A.: A biochemical model of photosynthetic CO2 assimilation in leaves of C3 species, Planta, 149, 78-90, https://doi.org/10.1007/BF00386231, 1980.

Fiore, A. M., Naik, V., and Leibensperger, E. M.: Air Quality and Climate Connections, J. Air Waste Manage. Assoc., 65, 645-685, https://doi.org/10.1080/10962247.2015.1040526, 2015.

Fiore, A. M., Naik, V., Spracklen, D. V., Steiner, A., Unger, N., Prather, M., Bergmann, D., Cameron-Smith, P. J., *et al.*: Global air quality and climate, Chem. Soc. Rev., 41, 6663-6683, https://doi.org/10.1039/c2cs35095e,

581    2012.

582    Forkel, M., Carvalhais, N., Rodenbeck, C., Keeling, R., Heimann, M., Thonicke, K., Zaehle, S., and Reichstein,
583        M.: Enhanced seasonal CO2 exchange caused by amplified plant productivity in northern ecosystems,
584        Science, 351, 696-699, https://doi.org/10.1126/science.aac4971, 2016.

585    Gao, Y. M., Zhuang, B. L., Wang, T. J., Chen, H. M., Li, S., Wei, W., Lin, H. J., and Li, M. M.:
586        Climatic-Environmental Effects of Aerosols and Their Sensitivity to Aerosol Mixing States in East Asia in
587        Winter, Remote Sens., 14, https://doi.org/10.3390/rs14153539, 2022.

588    Gery, M. W., Whitten, G. Z., Killus, J. P., and Dodge, M. C.: A Photochemical Kinetics Mechanism for Urban
589        and Regional Scale Computer Modeling, J. Geophys. Res.: Atmos., 94, 12925-12956,
590        https://doi.org/10.1029/JD094iD10p12925, 1989.

591    Giorgi, F.: Simulation of Regional Climate Using a Limited Area Model Nested in a General-Circulation Model,
592        J. Clim., 3, 941-963, https://doi.org/10.1175/1520-0442(1990)003<0941:Sorcua>2.0.Co;2, 1990.

593    Giorgi, F. and Bates, G. T.: The Climatological Skill of a Regional Model over Complex Terrain, Mon. Weather
594        Rev., 117, 2325-2347, https://doi.org/10.1175/1520-0493(1989)117<2325:TCSOAR>2.0.CO;2, 1989.

595    Giorgi, F. and Mearns, L. O.: Introduction to special section: Regional climate modeling revisited, J. Geophys.
596        Res.: Atmos., 104, 6335-6352, https://doi.org/10.1029/98jd02072, 1999.

597    Giorgi, F., Marinucci, M. R., Bates, G. T., and Decanio, G.: DEVELOPMENT OF A 2ND-GENERATION
598        REGIONAL CLIMATE MODEL (REGCM2) .2. CONVECTIVE PROCESSES AND ASSIMILATION OF
599        LATERAL BOUNDARY-CONDITIONS, Mon. Weather Rev., 121, 2814-2832,
600        https://doi.org/10.1175/1520-0493(1993)121<2814:Doasgr>2.0.Co;2, 1993.

601    Giorgi, F., Pal, J. S., Bi, X., Sloan, L., Elguindi, N., and Solmon, F.: Introduction to the TAC special issue: The
602        RegCNET network, Theor. Appl. Climatol., 86, 1-4, https://doi.org/10.1007/s00704-005-0199-z, 2006.

603    Giorgi, F., Coppola, E., Solmon, F., Mariotti, L., Sylla, M. B., Bi, X., Elguindi, N., Diro, G. T._, et al._: RegCM4:
604        model description and preliminary tests over multiple CORDEX domains, Clim. Res., 52, 7-29,
605        https://doi.org/10.3354/cr01018, 2012.

606    Guenther, A., Hewitt, C. N., Erickson, D., Fall, R., Geron, C., Graedel, T., Harley, P., Klinger, L._, et al._: A
607        Global-Model of Natural Volatile Organic-Compound Emissions, J. Geophys. Res.: Atmos., 100,
608        8873-8892, https://doi.org/10.1029/94jd02950, 1995.

609    Han, Z. W., Li, J. W., Xia, X. G., and Zhang, R. J.: Investigation of direct radiative effects of aerosols in dust
610        storm season over East Asia with an online coupled regional climate-chemistry-aerosol model, Atmos.
611        Environ., 54, 688-699, https://doi.org/10.1016/j.atmosenv.2012.01.041, 2012.

612    Han, Z. W., Xie, Z. X., Wang, G. H., Zhang, R. J., and Tao, J.: Modeling organic aerosols over east China using
613        a volatility basis-set approach with aging mechanism in a regional air quality model, Atmos. Environ., 124,
614        186-198, https://doi.org/10.1016/j.atmosenv.2015.05.045, 2016.

615    He, M. Z., Kimball, J. S., Maneta, M. P., Maxwell, B. D., Moreno, A., Begueria, S., and Wu, X. C.: Regional
616        Crop Gross Primary Productivity and Yield Estimation Using Fused Landsat-MODIS Data, Remote Sens.,
617        10, https://doi.org/10.3390/rs10030372, 2018.

618    Hong, C. P., Zhang, Q., Zhang, Y., Davis, S. J., Tong, D., Zheng, Y. X., Liu, Z., Guan, D. B._, et al._: Impacts of
619        climate change on future air quality and human health in China, Proc. Natl. Acad. Sci. U.S.A., 116,
620        17193-17200, https://doi.org/10.1073/pnas.1812881116, 2019.

621    Horowitz, L. W., Walters, S., Mauzerall, D. L., Emmons, L. K., Rasch, P. J., Granier, C., Tie, X. X., Lamarque, J.
622        F._, et al._: A global simulation of tropospheric ozone and related tracers: Description and evaluation of
623        MOZART, version 2, J. Geophys. Res.: Atmos., 108, https://doi.org/10.1029/2002jd002853, 2003.

624    Kan, H. D., Chen, R. J., and Tong, S. L.: Ambient air pollution, climate change, and population health in China,

625    Environ. Int., 42, 10-19, https://doi.org/10.1016/j.envint.2011.03.003, 2012.

626    Kiehl, J. T., Hack, J. J., Bonan, G. B., Boville, B. A., and Briegleb, B. P.: Description of the NCAR community
627        climate model (CCM3), National Center for Atmospheric Research, Boulder, CO (United States). Climate
628        and Global Dynamics Div., Technical Report PB-97-131528/XAB;NCAR/TN-420-STR TRN: 70341499,
629        1996.

630    Kim, K. H., Kabir, E., and Kabir, S.: A review on the human health impact of airborne particulate matter,
631        Environ. Int., 74, 136-143, https://doi.org/10.1016/j.envint.2014.10.005, 2015.

632    Kou, X. X., Zhang, M. G., Peng, Z., and Wang, Y. H.: Assessment of the biospheric contribution to surface
633        atmospheric $CO_2$ concentrations over East Asia with a regional chemical transport model, Adv. Atmos. Sci.,
634        32, 287-300, https://doi.org/10.1007/s00376-014-4059-6, 2015.

635    Lamarque, J. F., Dentener, F., McConnell, J., Ro, C. U., Shaw, M., Vet, R., Bergmann, D., Cameron-Smith, P., *et
636        al.*: Multi-model mean nitrogen and sulfur deposition from the Atmospheric Chemistry and Climate Model
637        Intercomparison Project (ACCMIP): evaluation of historical and projected future changes, Atmos. Chem.
638        Phys., 13, 7997-8018, https://doi.org/10.5194/acp-13-7997-2013, 2013.

639    Lawrence, P. J. and Chase, T. N.: Representing a new MODIS consistent land surface in the Community Land
640        Model (CLM 3.0), J. Geophys. Res.: Biogeosci., 112, https://doi.org/10.1029/2006jg000168, 2007.

641    Li, B., Gasser, T., Ciais, P., Piao, S., Tao, S., Balkanski, Y., Hauglustaine, D., Boisier, J.-P., *et al.*: The
642        contribution of China's emissions to global climate forcing, Nature, 531, 357-361,
643        https://doi.org/10.1038/nature17165, 2016a.

644    Li, J. W., Han, Z. W., and Xie, Z. X.: Model analysis of long-term trends of aerosol concentrations and direct
645        radiative forcings over East Asia, Tellus B: Chem. Phys. Meteorol., 65,
646        https://doi.org/10.3402/tellusb.v65i0.20410, 2013a.

647    Li, J. W., Han, Z. W., and Zhang, R. J.: Influence of aerosol hygroscopic growth parameterization on aerosol
648        optical depth and direct radiative forcing over East Asia, Atmos. Res., 140, 14-27,
649        https://doi.org/10.1016/j.atmosres.2014.01.013, 2014.

650    Li, M., Wang, T., Han, Y., Xie, M., Li, S., Zhuang, B., and Chen, P.: Modeling of a severe dust event and its
651        impacts on ozone photochemistry over the downstream Nanjing megacity of eastern China, Atmos.
652        Environ., 160, 107-123, https://doi.org/10.1016/j.atmosenv.2017.04.010, 2017a.

653    Li, M., Zhang, Q., Kurokawa, J., Woo, J. H., He, K. B., Lu, Z. F., Ohara, T., Song, Y., *et al.*: MIX: a mosaic
654        Asian anthropogenic emission inventory under the international collaboration framework of the MICS-Asia
655        and HTAP, Atmos. Chem. Phys., 17, 935-963, https://doi.org/10.5194/acp-17-935-2017, 2017b.

656    Li, S., Wang, T. J., Zhuang, B. L., and Han, Y.: Indirect radiative forcing and climatic effect of the anthropogenic
657        nitrate aerosol on regional climate of China, Adv. Atmos. Sci., 26, 543-552,
658        https://doi.org/10.1007/s00376-009-0543-9, 2009.

659    Li, S., Wang, T. J., Solmon, F., Zhuang, B. L., Wu, H., Xie, M., Han, Y., and Wang, X. M.: Impact of aerosols on
660        regional climate in southern and northern China during strong/weak East Asian summer monsoon years, J.
661        Geophys. Res.: Atmos., 121, 4069-4081, https://doi.org/10.1002/2015jd023892, 2016b.

662    Li, X. L., Liang, S. L., Yu, G. R., Yuan, W. P., Cheng, X., Xia, J. Z., Zhao, T. B., Feng, J. M., *et al.*: Estimation
663        of gross primary production over the terrestrial ecosystems in China, Ecol. Model., 261, 80-92,
664        https://doi.org/10.1016/j.ecolmodel.2013.03.024, 2013b.

665    Liu, L., Solmon, F., Vautard, R., Hamaoui-Laguel, L., Torma, C. Z., and Giorgi, F.: Ragweed pollen production
666        and dispersion modelling within a regional climate system, calibration and application over Europe,
667        Biogeosciences, 13, 2769-2786, https://doi.org/10.5194/bg-13-2769-2016, 2016.

668    Liu, Z., Deng, Z., He, G., Wang, H. L., Zhang, X., Lin, J., Qi, Y., and Liang, X.: Challenges and opportunities

for carbon neutrality in China, Nat Rev Earth Env, 3, 141-155, https://doi.org/10.1038/s43017-021-00244-x, 2022.

Lu, X., Zhang, S. J., Xing, J., Wang, Y. J., Chen, W. H., Ding, D., Wu, Y., Wang, S. X*., et al.*: Progress of Air Pollution Control in China and Its Challenges and Opportunities in the Ecological Civilization Era, Engineering, 6, 1423-1431, https://doi.org/10.1016/j.eng.2020.03.014, 2020.

Lu, X. L., Chen, M., Liu, Y. L., Miralles, D. G., and Wang, F. M.: Enhanced water use efficiency in global terrestrial ecosystems under increasing aerosol loadings, Agric. For. Meteorol., 237, 39-49, https://doi.org/10.1016/j.agrformet.2017.02.002, 2017.

Ma, D., Wang, T., Wu, H., Qu, Y., Liu, J., Liu, J., Li, S., Zhuang, B*., et al.*: The effect of anthropogenic emission, meteorological factors, and carbon dioxide on the surface ozone increase in China from 2008 to 2018 during the East Asia summer monsoon season, Atmos. Chem. Phys., 23, 6525-6544, https://doi.org/10.5194/acp-23-6525-2023, 2023a.

Ma, D. Y., Wang, T. J., Xu, B. Y., Song, R., Gao, L. B., Chen, H. M., Ren, X. J., Li, S*., et al.*: The mutual interactions among ozone, fine particulate matter, and carbon dioxide on summer monsoon climate in East Asia, Atmos. Environ., 299, https://doi.org/10.1016/j.atmosenv.2023.119668, 2023b.

Madani, N., Kimball, J. S., Affleck, D. L. R., Kattge, J., Graham, J., van Bodegom, P. M., Reich, P. B., and Running, S. W.: Improving ecosystem productivity modeling through spatially explicit estimation of optimal light use efficiency, J. Geophys. Res.: Biogeosci., 119, 1755-1769, https://doi.org/10.1002/2014jg002709, 2014.

Madronich, S. and Flocke, S.: The role of solar radiation in atmospheric chemistry, Environ. Chem., 1-26, https://doi.org/10.1007/978-3-540-69044-3_1, 1998.

Niinemets, Ü., Tenhunen, J. D., Harley, P. C., and Steinbrecher, R.: A model of isoprene emission based on energetic requirements for isoprene synthesis and leaf photosynthetic properties for Liquidambar and Quercus, Plant, Cell & Environment, 22, 1319-1335, https://doi.org/10.1046/j.1365-3040.1999.00505.x, 2002.

Oleson, K. W., Niu, G. Y., Yang, Z. L., Lawrence, D. M., Thornton, P. E., Lawrence, P. J., Stockli, R., Dickinson, R. E*., et al.*: Improvements to the Community Land Model and their impact on the hydrological cycle, J. Geophys. Res.: Biogeosci., 113, https://doi.org/10.1029/2007jg000563, 2008.

Pacifico, F., Harrison, S. P., Jones, C. D., Arneth, A., Sitch, S., Weedon, G. P., Barkley, M. P., Palmer, P. I., et al.: Evaluation of a photosynthesis-based biogenic isoprene emission scheme in JULES and simulation of isoprene emissions under present-day climate conditions, Atmos. Chem. Phys., 11, 4371-4389, https://doi.org/10.5194/acp-11-4371-2011, 2011.

Pal, J. S., Giorgi, F., Bi, X. Q., Elguindi, N., Solmon, F., Gao, X. J., Rauscher, S. A., Francisco, R*., et al.*: Regional climate modeling for the developing world - The ICTP RegCM3 and RegCNET, Bull. Am. Meteorol. Soc., 88, 1395-+, https://doi.org/10.1175/Bams-88-9-1395, 2007.

Peters, W., Jacobson, A. R., Sweeney, C., Andrews, A. E., Conway, T. J., Masarie, K., Miller, J. B., Bruhwiler, L. M. P*., et al.*: An atmospheric perspective on North American carbon dioxide exchange: CarbonTracker, Proc. Natl. Acad. Sci. U.S.A., 104, 18925-18930, https://doi.org/10.1073/pnas.0708986104, 2007.

Pu, X., Wang, T. J., Huang, X., Melas, D., Zanis, P., Papanastasiou, D. K., and Poupkou, A.: Enhanced surface ozone during the heat wave of 2013 in Yangtze River Delta region, China, Sci. Total Environ., 603, 807-816, https://doi.org/10.1016/j.scitotenv.2017.03.056, 2017.

Reynolds, R. W., Rayner, N. A., Smith, T. M., Stokes, D. C., and Wang, W. Q.: An improved in situ and satellite SST analysis for climate, J. Clim., 15, 1609-1625, https://doi.org/10.1175/1520-0442(2002)015<1609:Aiisas>2.0.Co;2, 2002.

Running, S. W.: A Measurable Planetary Boundary for the Biosphere, Science, 337, 1458-1459, https://doi.org/10.1126/science.1227620, 2012.

Scheuch, M., Hoper, D., and Beer, M.: RIEMS: a software pipeline for sensitive and comprehensive taxonomic classification of reads from metagenomics datasets, BMC Bioinf., 16, https://doi.org/10.1186/s12859-015-0503-6, 2015.

Shalaby, A., Zakey, A. S., Tawfik, A. B., Solmon, F., Giorgi, F., Stordal, F., Sillman, S., Zaveri, R. A*., et al.*: Implementation and evaluation of online gas-phase chemistry within a regional climate model (RegCM-CHEM4), Geosci. Model Dev., 5, 741-760, https://doi.org/10.5194/gmd-5-741-2012, 2012.

Shindell, D. T., Lamarque, J. F., Schulz, M., Flanner, M., Jiao, C., Chin, M., Young, P. J., Lee, Y. H*., et al.*: Radiative forcing in the ACCMIP historical and future climate simulations, Atmos. Chem. Phys., 13, 2939-2974, https://doi.org/10.5194/acp-13-2939-2013, 2013.

Sitch, S., Cox, P. M., Collins, W. J., and Huntingford, C.: Indirect radiative forcing of climate change through ozone effects on the land-carbon sink, Nature, 448, 791-U794, https://doi.org/10.1038/nature06059, 2007.

Slingo, A.: A Gcm Parameterization for the Shortwave Radiative Properties of Water Clouds, J. Atmos. Sci., 46, 1419-1427, https://doi.org/10.1175/1520-0469(1989)046<1419:Agpfts>2.0.Co;2, 1989.

Small, E. E., Sloan, L. C., Hostetler, S., and Giorgi, F.: Simulating the water balance of the Aral Sea with a coupled regional climate-lake model, J. Geophys. Res.: Atmos., 104, 6583-6602, https://doi.org/Doi 10.1029/98jd02348, 1999.

Solmon, F., Elguindi, N., and Mallet, M.: Radiative and climatic effects of dust over West Africa, as simulated by a regional climate model, Clim. Res., 52, 97-113, https://doi.org/10.3354/cr01039, 2012.

Solmon, F., Giorgi, F., and Liousse, C.: Aerosol modelling for regional climate studies: application to anthropogenic particles and evaluation over a European/African domain, Tellus B: Chem. Phys. Meteorol., 58, 51-72, https://doi.org/10.1111/j.1600-0889.2005.00155.x, 2006.

Spitters, C. J. T., Toussaint, H., and Goudriaan, J.: SEPARATING THE DIFFUSE AND DIRECT COMPONENT OF GLOBAL RADIATION AND ITS IMPLICATIONS FOR MODELING CANOPY PHOTOSYNTHESIS .1. COMPONENTS OF INCOMING RADIATION, Agric. For. Meteorol., 38, 217-229, https://doi.org/10.1016/0168-1923(86)90060-2, 1986.

Strada, S. and Unger, N.: Potential sensitivity of photosynthesis and isoprene emission to direct radiative effects of atmospheric aerosol pollution, Atmos. Chem. Phys., 16, 4213-4234, https://doi.org/10.5194/acp-16-4213-2016, 2016.

Turuncoglu, U. U., Dalfes, N., Murphy, S., and DeLuca, C.: Toward self-describing and workflow integrated Earth system models: A coupled atmosphere-ocean modeling system application, Environ. Model. Software, 39, 247-262, https://doi.org/10.1016/j.envsoft.2012.02.013, 2013.

Wang, T., Xue, L. K., Brimblecombe, P., Lam, Y. F., Li, L., and Zhang, L.: Ozone pollution in China: A review of concentrations, meteorological influences, chemical precursors, and effects, Sci. Total Environ., 575, 1582-1596, https://doi.org/10.1016/j.scitotenv.2016.10.081, 2017.

Wang, T. J., Li, S., Shen, Y., Deng, J. J., and Xie, M.: Investigations on direct and indirect effect of nitrate on temperature and precipitation in China using a regional climate chemistry modeling system, J. Geophys. Res.: Atmos., 115, https://doi.org/10.1029/2009jd013264, 2010.

Wesely, M. L.: Parameterization of Surface Resistances to Gaseous Dry Deposition in Regional-Scale Numerical-Models, Atmos. Environ., 23, 1293-1304, https://doi.org/10.1016/0004-6981(89)90153-4, 1989.

Wiedinmyer, C., Akagi, S. K., Yokelson, R. J., Emmons, L. K., Al-Saadi, J. A., Orlando, J. J., and Soja, A. J.: The Fire INventory from NCAR (FINN): a high resolution global model to estimate the emissions from open burning, Geosci. Model Dev., 4, 625-641, https://doi.org/10.5194/gmd-4-625-2011, 2011.

Xie, X. D., Wang, T. J., Yue, X., Li, S., Zhuang, B. L., and Wang, M. H.: Effects of atmospheric aerosols on terrestrial carbon fluxes and CO2 concentrations in China, Atmos. Res., 237, https://doi.org/10.1016/j.atmosres.2020.104859, 2020.

Xie, X. D., Wang, T. J., Yue, X., Li, S., Zhuang, B. L., Wang, M. H., and Yang, X. Q.: Numerical modeling of ozone damage to plants and its effects on atmospheric CO2 in China, Atmos. Environ., 217, https://doi.org/10.1016/j.atmosenv.2019.116970, 2019.

Xiong, Z., Fu, C. B., and Yan, X. D.: Regional integrated environmental model system and its simulation of East Asia summer monsoon, Chin. Sci. Bull., 54, 4253-4261, https://doi.org/10.1007/s11434-009-0669-2, 2009.

Xu, B. Y., Wang, T. J., Ma, D. Y., Song, R., Zhang, M., Gao, L. B., Li, S., Zhuang, B. L., *et al.*: Impacts of regional emission reduction and global climate change on air quality and temperature to attain carbon neutrality in China, Atmos. Res., 279, https://doi.org/10.1016/j.atmosres.2022.106384, 2022.

Xu, B. Y., Wang, T. J., Gao, L. B., Ma, D. Y., Song, R., Zhao, J., Yang, X. G., Li, S., *et al.*: Impacts of meteorological factors and ozone variation on crop yields in China concerning carbon neutrality objectives in 2060, Environ. Pollut., 317, https://doi.org/10.1016/j.envpol.2022.120715, 2023.

Yahya, K., Wang, K., Campbell, P., Chen, Y., Glotfelty, T., He, J., Pirhalla, M., and Zhang, Y.: Decadal application of WRF/Chem for regional air quality and climate modeling over the U.S. under the representative concentration pathways scenarios. Part 1: Model evaluation and impact of downscaling, Atmos. Environ., 152, 562-583, https://doi.org/10.1016/j.atmosenv.2016.12.029, 2017.

Yin, C. Q., Wang, T. J., Solmon, F., Mallet, M., Jiang, F., Li, S., and Zhuang, B. L.: Assessment of direct radiative forcing due to secondary organic aerosol over China with a regional climate model, Tellus Series B-Chemical and Physical Meteorology, 67, https://doi.org/10.3402/tellusb.v67.24634, 2015.

Yin, J. F., Wang, D. H., Zhai, G. Q., and Xu, H. B.: An investigation into the relationship between liquid water content and cloud number concentration in the stratiform clouds over north China, Atmos. Res., 139, 137-143, https://doi.org/10.1016/j.atmosres.2013.12.004, 2014.

Young, P. J., Archibald, A. T., Bowman, K. W., Lamarque, J. F., Naik, V., Stevenson, D. S., Tilmes, S., Voulgarakis, A., *et al.*: Pre-industrial to end 21st century projections of tropospheric ozone from the Atmospheric Chemistry and Climate Model Intercomparison Project (ACCMIP), Atmos. Chem. Phys., 13, 2063-2090, https://doi.org/10.5194/acp-13-2063-2013, 2013.

Yue, X. and Unger, N.: The Yale Interactive terrestrial Biosphere model version 1.0: description, evaluation and implementation into NASA GISS ModelE2, Geosci. Model Dev., 8, 2399-2417, https://doi.org/10.5194/gmd-8-2399-2015, 2015.

Yue, X. and Unger, N.: Aerosol optical depth thresholds as a tool to assess diffuse radiation fertilization of the land carbon uptake in China, Atmos. Chem. Phys., 17, 1329-1342, https://doi.org/10.5194/acp-17-1329-2017, 2017.

Yue, X., Strada, S., Unger, N., and Wang, A. H.: Future inhibition of ecosystem productivity by increasing wildfire pollution over boreal North America, Atmos. Chem. Phys., 17, 13699-13719, https://doi.org/10.5194/acp-17-13699-2017, 2017.

Zakey, A. S., Solmon, F., and Giorgi, F.: Implementation and testing of a desert dust module in a regional climate model, Atmos. Chem. Phys., 6, 4687-4704, https://doi.org/10.5194/acp-6-4687-2006, 2006.

Zaveri, R. A. and Peters, L. K.: A new lumped structure photochemical mechanism for large-scale applications, J. Geophys. Res.: Atmos., 104, 30387-30415, https://doi.org/10.1029/1999jd900876, 1999.

Zhang, H., Jing, X., and Li, J.: Application and evaluation of a new radiation code under McICA scheme in BCC_AGCM2.0.1, Geosci. Model Dev., 7, 737-754, https://doi.org/10.5194/gmd-7-737-2014, 2014.

Zhang, H., Wang, Z. L., Wang, Z. Z., Liu, Q. X., Gong, S. L., Zhang, X. Y., Shen, Z. P., Lu, P., *et al.*: Simulation

of direct radiative forcing of aerosols and their effects on East Asian climate using an interactive AGCM-aerosol coupled system, Clim. Dyn., 38, 1675-1693, https://doi.org/10.1007/s00382-011-1131-0, 2012.

Zheng, B., Tong, D., Li, M., Liu, F., Hong, C. P., Geng, G. N., Li, H. Y., Li, X.*, et al.*: Trends in China's anthropogenic emissions since 2010 as the consequence of clean air actions, Atmos. Chem. Phys., 18, 14095-14111, https://doi.org/10.5194/acp-18-14095-2018, 2018.

Zhou, Y., Huang, A. N., Jiang, J., and La, M. K.: Modeled interaction between the subseasonal evolving of the East Asian summer monsoon and the direct effect of anthropogenic sulfate, J. Geophys. Res.: Atmos., 119, 1993-2016, https://doi.org/10.1002/2013jd020612, 2014.

Zhuang, B. L., Jiang, F., Wang, T. J., Li, S., and Zhu, B.: Investigation on the direct radiative effect of fossil fuel black-carbon aerosol over China, Theor. Appl. Climatol., 104, 301-312, https://doi.org/10.1007/s00704-010-0341-4, 2011.

Zhuang, B. L., Li, S., Wang, T. J., Deng, J. J., Xie, M., Yin, C. Q., and Zhu, J. L.: Direct radiative forcing and climate effects of anthropogenic aerosols with different mixing states over China, Atmos. Environ., 79, 349-361, https://doi.org/10.1016/j.atmosenv.2013.07.004, 2013.

Zhuang, B. L., Li, S., Wang, T. J., Liu, J., Chen, H. M., Chen, P. L., Li, M. M., and Xie, M.: Interaction between the Black Carbon Aerosol Warming Effect and East Asian Monsoon Using RegCM4, J. Clim., 31, 9367-9388, https://doi.org/10.1175/Jcli-D-17-0767.1, 2018.